JOURNAL OF THERMOPHYSICS AND HEAT TRANSFER
Vol. 23, No. 3, July–September 2009

Cooling Performance of a 16-Nozzle Array in Variable Gravity

Levi J. Elston* and Kirk L. Yerkes†
U.S. Air Force Research Laboratory, Wright–Patterson Air Force Base, Ohio 45433
Scott K. Thomas‡
Wright State University, Dayton, Ohio 45435
and
John McQuillen§
NASA John H. Glenn Research Center at Lewis Field, Cleveland, Ohio 44135

DOI: 10.2514/1.41653

The objective of this paper was to investigate the cooling performance of a 16-nozzle spray array using FC-72 as the working fluid in variable-gravity conditions. A flight-test experiment was modified to accommodate a 16-nozzle spray array, which was then tested in the parabolic flight trajectory environment of NASA's C-9 reduced-gravity aircraft. The 16-nozzle array was designed to cool a 25.4 × 25.4 mm² area on a thick-film resistive heater used to simulate an electronic component. Flight tests were conducted over the course of two flight weeks (each week consisting of four flights and each flight consisting of 40 to 60 parabolas). The mass flow rate through the 16-nozzle spray array ranged from $13.1 \le \dot{m} \le 21.3$ g/s. The heat flux at the thick-film resistor ranged from $2.9 \le q'' \le 25$ W/cm², the subcooling of the working fluid ranged from $1.6 \le \Delta T_{sc} \le 18.4$°C, the saturation temperature ranged from $37.4 \le T_{sat} \le 47.2$°C, and the absorbed air content in the working fluid was $C = 10.1$, 14.3 and 16.8% by volume. The spray chamber pressure ranged from $42 \le P \le 78$ kPa and the acceleration ranged from $-0.02 \le a \le -2.02\ g$. Two-phase cooling was emphasized, but some single-phase data were also collected. A one-dimensional model was used to predict the heater surface temperature from the heat input and mean heater base temperature. It was found that the cooling performance was enhanced in microgravity over terrestrial and elevated gravity. In addition, a sudden degradation in performance was found at high mass flow rates in microgravity, possibly due to liquid buildup on the surface between the nozzle impact zones. A high degree of subcooling was found to be beneficial, but the dissolved air content had little effect on the heat transfer performance in either microgravity or elevated gravity.

Nomenclature

A	=	area, m²
a	=	acceleration, m/s²
C	=	percent of dissolved air content by volume, $[V_{air}/(V_{FC\text{-}72} + V_{air})] \times 100$
D	=	mean droplet diameter, m
Fr	=	Froude number, v^2/aD
f	=	fraction of heat lost down the pedestal
Ga	=	Galileo number, $aD^3\rho^2/\mu^2$
$G\Delta$	=	nondimensional heat input, $Q/[2k_rW(T_{sat} - T_\infty)]$
k	=	thermal conductivity, W/(m · K)
L	=	heater layer thickness, m
$\dot{m}$	=	mass flow rate, kg/s
P	=	chamber pressure, kPa
Q	=	heat rate, W
q''	=	heat flux, W/m²
T	=	temperature, K
$\bar{T}$	=	average temperature, K
V	=	volume, m³
v	=	droplet velocity, m/s
W	=	heater width, m
We	=	Weber number, $\rho v^2 D/\sigma$
ΔT	=	temperature difference, K
μ	=	viscosity, Pa · s
ρ	=	density, kg/m³
σ	=	surface tension, N/m, or standard deviation
θ	=	nondimensional temperature, $(T - T_{\infty,surf})/(T_{sat} - T_{\infty,surf})$

Subscripts

c	=	heater ceramic layer (substrate)
g	=	heater glass layer (cover plate)
in	=	nozzle inlet
int	=	interface between phenolic base and bottom of heater
r	=	heater resistive layer
sat	=	saturated condition
sc	=	subcooling
surf	=	heater surface exposed to spray
∞	=	freestream condition

Received 16 October 2008; revision received 20 January 2009; accepted for publication 4 February 2009.

*Mechanical Engineer, Thermal and Electrochemical Branch, 1950 Fifth Street, Building 18. Member AIAA.
†Research Engineer, Deputy for Science, Energy/Power/Thermal Division, 1950 Fifth Street, Building 18. Senior Member AIAA.
‡Associate Professor, Department of Mechanical and Materials Engineering, Associate Fellow AIAA.
§Aerospace Engineer, Microgravity Fluid Physics Branch.

I. Introduction

THE increasing need for high-power electronic devices drives thermal management demands due to the inefficiency of electronic components and high-density device packaging. Large amounts of excess heat at high fluxes must be removed, transported, and rejected to an ambient environment using advanced thermal management approaches. High-power technologies often need active cooling methods to remove heat effectively and keep component reliability, usable life, and operability high. Passive methods such as heat pipes, thermal radiation, and natural convection using

enhanced surfaces can be used if the heat flux is small. When higher heat fluxes are generated, active cooling techniques must be used to prevent component failure. Many of these techniques, such as single-phase forced convection, pool boiling, flow boiling, jet impingement, and spray cooling, have been studied in depth and are currently being used on various types of systems. Mudawar [1] presented many of the higher-heat-flux cooling schemes and ranked their heat transfer attainability, showing that under terrestrial gravity, two-phase convection can provide two- to three-orders-of-magnitude higher heat transfer coefficients over single-phase convection in addition to maintaining closer temperature tolerances.

Many of these technologies have also been investigated in a microgravity environment. For instance, Lee et al. [2] investigated the critical heat flux (CHF) and pool boiling curves for R-113 onboard the space shuttle, demonstrating a reduction in critical heat flux in microgravity. On the other hand, pulsating heat pipes, examined by Gu et al. [3], showed an improvement in heat transfer performance in microgravity. Kim [4] reviewed the state of the art in reduced-gravity boiling research, concluding that many parameters (electric fields, acoustic fields, flow boiling, and noncondensible gases) can affect performance, but the mechanisms of the studied parameters are still relatively unclear. The current research concentrated on spray cooling.

Spray cooling is a very promising technology with exceptional versatility in which many parameters can be adjusted to fit the needs of the application. Spray cooling is considered one of the most effective methods of high-flux-heat removal, because the latent heat of vaporization absorbs large amounts of heat with a minimal change in temperature. There are two types of spray cooling: pressure-atomized and vapor-atomized. In a pressure-atomized spray cooling system, liquid is pumped through a spray nozzle that is designed, using a swirler, to not only generate a spray cone, but to also atomize the droplets into an even distribution onto the sprayed surface. In a vapor-atomized spray cooling system, pressurized vapor is introduced into the pressurized liquid flow just before the liquid reaches the nozzle. The vapor atomizes the liquid into droplets without the use of a swirler.

Many factors contribute to the effectiveness of a spray cooling system, such as mass flow rate, array nozzle spacing, and subcooling. The phenomena and processes that are involved in spray cooling are not completely understood, but the thin liquid film formed on the heated surface plays an important role. The thickness of this film varies both spatially and temporally. As nucleation occurs on the surface, bubbles grow and eventually burst, perhaps from excessive size or droplet impact, creating a very short period during which the local film is made up entirely of vapor until new spray droplets can rewet the surface. In an array of spray nozzles, interactions occur that generate uneven film-thickness zones. Glassman et al. [5] investigated ways to reduce the liquid buildup between spray cones by placing suction tubes in these areas, thereby increasing the overall heat transfer by reducing the thickness of the liquid film. The effects of bubble growth, coalescence, and popping were all seen to play a significant role.

Many aspects of spray cooling have been investigated experimentally and numerically, including mass flow rate, subcooling, different working fluids, binary fluid mixtures, single nozzle or nozzle arrays, surface roughness, flow rate, and nozzle orientation [6]. Ortiz and Gonzalez [7] investigated the effects of mass flow rate, surface roughness, degree of subcooling, and impact angle for steady-state and transient conditions. Johnson et al. [8] numerically examined the effect of subcooling and how it enhances the critical heat flux. Selvam and Ponnappan [9] and Selvam et al. [10–13] numerically modeled the vapor bubble dynamics as a function of surface tension, gravity, phase change, and viscosity as a follow-up to previous numerical spray cooling work, including thin-film effects, nucleate boiling, droplet impact, droplet velocity, droplet interaction, and droplet density. The effect of dissolved air content on spray cooling performance was investigated by Puterbaugh et al. [14] and Puterbaugh [15]. Specifically, the sensitivity of CHF with air content was examined for a single nozzle in a terrestrial environment. The results of Puterbaugh et al. [14] and Puterbaugh [15] suggested that the amount of dissolved air in FC-72 has an insignificant effect on CHF. Kreitzer and Kuhlman [16], Kreitzer [17] and Kreitzer et al. [16–18] investigated body force effects on spray cooling by applying an electrostatic force to the spray cone, demonstrating small changes in heat transfer performance under specific conditions. Additionally, Glaspell [19] applied a magnetic field to the spray, achieving results that provided a maximum heat transfer improvement of 5.2% at a 6 kV electrode voltage.

Critical heat flux is the amount of heat at which the heat removal ability of the spray is exceeded and is a very important design criterion in a spray cooling system. Chow et al. [20] discussed the experimental background and macrolayer dryout model associated with CHF, suggesting an empirical correlation in which CHF can be determined using only the Sauter mean diameter of the spray droplets. Lin and Ponnappan [21] investigated CHF of various fluids including FC-72, FC-87, methanol, and water. Lin and Ponnappan [22] and Lin et al. [23] examined orientation effects (heated surfaces, both vertical and horizontal, with the spray facing upward) of a 48-nozzle array using FC-72, in which a 5% increase in CHF, in the horizontal-surface case, over the vertical heated surface was demonstrated. Lin et al. [24] explored the spray cooling performance of a binary fluid (50% methanol and 50% water) to reduce the freezing point of water to -40°C while maintaining convective performance near that of water.

Sone et al. [25] investigated the effects of reduced and elevated gravity on spray cooling using water and FC-72 on a MU-300 aircraft. Two separate experiments were conducted, each using the same nonrecirculating flow loop that pumped fluid using a pressurized syringe of liquid. Experimental difficulties arose during flight testing that restricted the amount of droplet velocity data obtained, although the data did suggest up to a 20% increase in droplet velocity in reduced gravity.

The first experimental apparatus used by Sone et al. [25] consisted of a copper block heater with a polished and chrome-plated cooling face, with the gravity vector normal to this face. These experiments operated in a transient cooling mode in which the block was heated to a certain temperature, the heat was turned off, and the spray cooled the block during each parabola. At low flow rates, water showed no distinguishable difference in performance, but at higher flow rates, the reduced-gravity test showed a significant reduction in cooling performance. FC-72, on the other hand, resulted in a substantial increase in CHF (14%) and reduction in wall superheat in the reduced-gravity test.

The second experimental apparatus used by Sone et al. [25] was an optically transparent indium tin oxide (ITO) heater that allowed for flow visualization during the flight test. The experiments were conducted in a steady-state operation mode in which the heat flux was held constant during the parabola. Using water as a coolant, a slight degradation in cooling performance (10% decrease in CHF) was observed in the reduced-gravity environment as opposed to the elevated gravity. No parabolic tests using FC-72 were completed with the transparent heater.

Yoshida et al. [26] further investigated effects of gravity on spray cooling performance using a heated copper block and ITO heaters in a nonrecirculating flow loop. The work of Yoshida et al. [26] was an extension of the work done by Sone et al. [25] and therefore used the same experimental setup. The flight-test experiments showed an increase in CHF (10%) for testing with water in microgravity, which contradicted the results of Sone et al. [25], whereas with FC-72 in microgravity, Yoshida et al. [26] showed insignificant differences in CHF.

Baysinger et al. [27] began investigations of microgravity spray cooling in the United States using the NASA KC-135 reduced-gravity aircraft. An experiment was assembled to investigate gravity effects on a single nozzle spraying FC-72 onto a circular ITO heater mounted atop a cylindrical glass rod. Thermocouples were placed beneath the heater and a one-dimensional heat conduction analysis was conducted to estimate the surface temperature. Significant surface tension flow was observed in and around the nozzle, containment cap, and chamber walls. In microgravity, the surface tension forces became dominant not only in the spray chamber, but also in the

fluid reservoir. This caused significant flow rate dropouts that led to heater temperature spikes. These flow variations were also noticed in elevated-gravity conditions, but not necessarily for the same reasons: perhaps an additional pumping head existed due to flow-loop elevation differences. As an extension to this experimental work, Baysinger [28] numerically modeled the ITO heater and glass post under terrestrial-gravity conditions.

The experimental setup by Yerkes et al. [29] is very similar to that described by Baysinger et al. [27]. A significant change in the experimental setup was related to improving fluid management and control: a screen was added to the chamber annulus for fluid condensation and containment. Their results demonstrated a decreasing Nusselt number as the nondimensional grouping $(Fr^{1/2}Ga)^{1/2}\tan$ increased, suggesting that the heat transfer coefficient was higher in microgravity than in terrestrial or elevated gravity.

More recently, Michalak et al. [30] further investigated the effect of variable gravity on spray cooling performance, making more modifications to the experimental setup described by both Baysinger et al. [27] and Baysinger [28] and Yerkes et al. [29]. This included changing to a thick-film resistive heater that provided the capability to reach higher superheat temperatures without causing damage to the heater. The flight-test results showed similar trends to those presented by Yerkes et al. [29]: at a constant heat flux, the heater surface temperature was reduced as the gravitational body force decreased, for all flow rates and subcooling amounts examined. The data from Michalak et al. [30] also contained partial-gravity tests: lunar ($a = -1/6\ g$) and Martian ($a = -1/3\ g$). Although the cooling performance enhancement for the partial-gravity tests was not as great as the microgravity case, an improvement was still apparent. The amount of subcooling in the spray also showed an effect demonstrating an enhancement in the reduced acceleration effect with increasing subcooling. Neither Baysinger et al. [27,28], Yerkes et al. [29], nor Michalak et al. [30] investigated acceleration effects on CHF. In addition, they did not track the amount of dissolved air in the test apparatus.

Gambaryan-Roisman et al. [31] also explored the effect of gravity on a single-nozzle open-loop spray cooling system that provided pressurized water to spray onto a convex heated surface. The work was completed to primarily investigate the film-thickness effects on cooling performance in microgravity and the liquid–vapor interface effects of the impacting spray. The parabolic flight tests additionally demonstrated a noticeable decrease in heat transfer in microgravity that most likely was due to a thickening film in the absence of gravity. The convex surface used the presence of gravity to assist in drainage, contributing to a thinner liquid film, deeper droplet penetration, and an increase in heat transfer.

It has been assumed that the high momentum flux of droplets impinging upon a heated surface drives the heat transfer and CHF, such that body forces were assumed not to play a significant role in heat transfer [6]. Previous research has shown that many factors contribute to the cooling performance of a spray cooling system and it is difficult to isolate a single parameter. Additionally, single-nozzle spray cooling under variable-gravity research has shown that, depending on the working fluid, geometry, and various operating conditions, the cooling performance in microgravity can be noticeably higher than in accelerations greater than $a = -1.0\ g$. Finally, research involving spray arrays in a variable-gravity environment does not exist in the archival literature. The present work investigated various parameters that affect the cooling performance of a 16-nozzle spray array in variable-gravity conditions. The objective of the flight-test experiment was to show the effects of gravity, flow rate, liquid subcooling, and dissolved air content on array spray cooling performance under the following parameter ranges: $13.1 \le \dot{m} \le 21.3$ g/s, $2.9 \le q'' \le 25$ W/cm^2, $1.6 \le \Delta T_{sc} \le 18.4$°C, $37.4 \le T_{sat} \le 47.2$°C, $C = 10.1$, 14.3 and 16.8%, $42 \le P \le 78$ kPa, and $-0.02 \le a \le -2.02\ g$.

II. Experimental Setup

The 16-nozzle spray array experiment consisted of five major components: the support structure, array spray chamber, liquid–vapor separator, heat rejection loop, and data acquisition system. The experiment was designed to fit in a package that would contain all necessary components while maintaining safety requirements and functionality in a variable-gravity environment. A test equipment data package was generated by Elston [32] according to the guidelines set by NASA [33], which define the standards to design, construct, and qualify a reduced-gravity flight-test experiment. The support structure was designed to meet NASA structural requirements while allowing accessibility to modify components throughout the system. The array spray chamber contained 16 individual spray nozzles, a resistive heater, and a wick-sump system. The liquid–vapor separator ensured that only liquid was introduced to the nozzle inlet. The heat rejection system recirculated the working fluid, FC-72, that acquired, transported, and rejected heat. Finally, the data acquisition system recorded data from all of the devices in the system and performed fault monitoring and control indication.

Each of the components was a part of an existing experimental setup [27–30] that was designed to fly onboard the NASA C-9 reduced-gravity platform. Modifications were made to accommodate the spray array. First, the single-nozzle spray chamber was replaced with a much smaller, lightweight, 16-nozzle array chamber. Second, a 1000 W power supply was mounted for the extra power required for the larger area heater, and additional temperature cutoffs were installed to monitor for spikes in the heater temperature distribution. Finally, due to the preceding modifications, the structure was reevaluated for strength and flightworthiness.

The design of the experiment was such that the overall cargo footprint was minimized while keeping the total height well below a standard "standing" operating level. The experiment size was restricted by the cargo door size on the aircraft. The experiment also had to be able to plug directly into the power outlets onboard the aircraft (110 Vac). The total experimental weight, nearly 320 kg, was in part due to the stringent structural requirements that required the experimental package, including each individual component, to be able to withstand the directional loading specified by NASA [33]. A factor of safety of two was applied to increase the margin of error. Pull tests using a load cell (Imada DPS-110) were completed on all components at a loading of up to 18 g.

The experimental package framework was designed starting with a $12.7 \times 1219.2 \times 1830$ mm^3 aluminum base plate. The rigidity of the frame came from the network of T-slotted aluminum extrusions (80/20, Inc.). Extrusion/bracket tests were performed to determine their strength when the frame integrity analysis was conducted. In addition, a step-by-step analysis was completed to determine how best to attach the rig to the airplane by determining the number of bolts and their placement, in accordance with the bolting grid defined by NASA. Elston [32] completed a detailed analysis of the support structure as a requirement for flight onboard the aircraft.

The 16-nozzle array and chamber are shown in Fig. 1. The spray chamber housed the 16-nozzle array, thick-film resistive (TFR) heater, aluminum foam surround, a pressure transducer port, and seven thermocouples. Liquid FC-72 entered the 16-nozzle assembly through a plenum via a 6.35 mm port atop the acrylic case. Liquid droplets were sprayed onto the TFR heater mounted to the phenolic base. Previous experience in using spray cooling systems in microgravity suggested the use of a wicking structure to aid in fluid management and retention of spray cooling systems. Any deflected liquid was then wicked into the aluminum foam surround, shown in Fig. 1c, which was machined to fill the volume that was not directly between the nozzle head and the heated surface. The foam provided an inlet to the scavenge ports while reducing the amount of liquid pooling on the heater surface. During reduced gravity, surface tension forces resulted in the liquid collecting within the foam structure, allowing for the liquid to flow out the exit ports.

The enclosure was sealed to the acrylic case with a compressed o-ring. The outer dimensions of the chamber were $87.9 \times 109.2 \times 76.2$ mm^3, with a wall thickness of 15.24 mm. The nozzle array head consisted of 16 individual nozzles, covering a 25.4×25.4 mm^2 area. The individual nozzles were assembled in a four-by-four array with 6 mm even spacing. No attempt was made to optimize the 16-nozzle array with respect to spacing. Each individual nozzle operated by

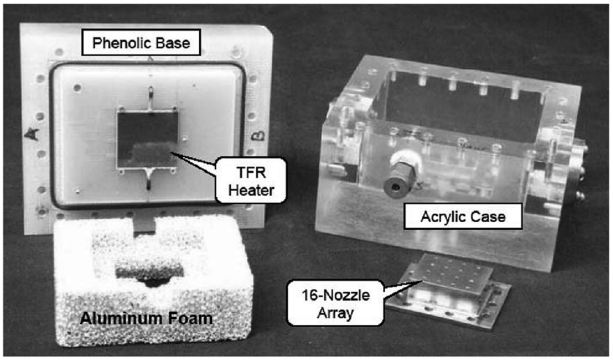

a)

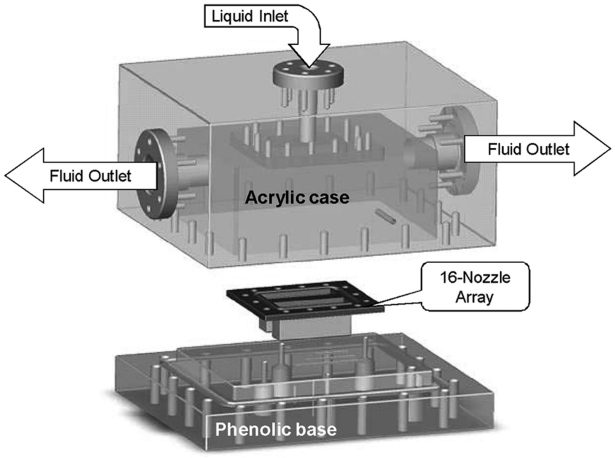

b)

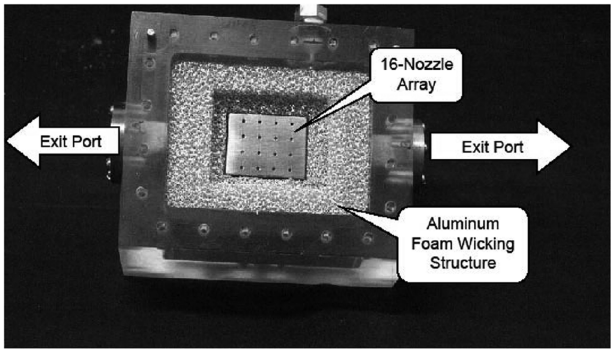

c)

Fig. 1 Array spray chamber: a) disassembled, b) three-dimensional array spray chamber design, and c) upper portion of the spray chamber.

passing liquid through a swirler that rotated the fluid centrifugally so that when the fluid entered the sapphire orifice (Bird Precision), a spray cone was generated. The exit of the nozzle plate was located 21.2 mm from the heated surface being sprayed.

A single nozzle was characterized using a phase Doppler anemometer. Droplet diameter, Sauter mean diameter, and droplet velocity were recorded for the desired range of flow rates and pressure drops. Functional relationships for both droplet diameter and droplet velocity as a function of flow rate were determined using a fourth-order polynomial fit, as shown in Fig. 2. Elston [32] presented additional nozzle characterization plots.

Heat was generated using a thick-film resistor (Mini Systems, Inc.) with an area of 25.4×25.4 mm^2. The heater was made of a deposited polymer film (resistive layer) sandwiched between a glass cover plate (sprayed surface) and an insulating substrate (ceramic layer). Thicknesses and thermal conductivities of each layer are shown in Table 1. Electrical connections to the heater were made by soldering a 0.127 mm nickel strap to the heater connection pads. The nickel strap allowed for flexibility from thermal expansion while

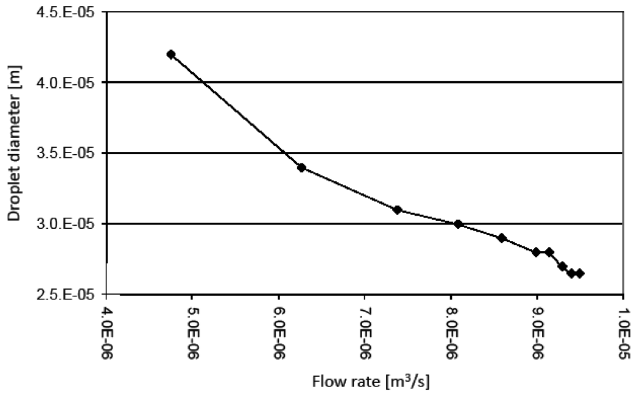

a)

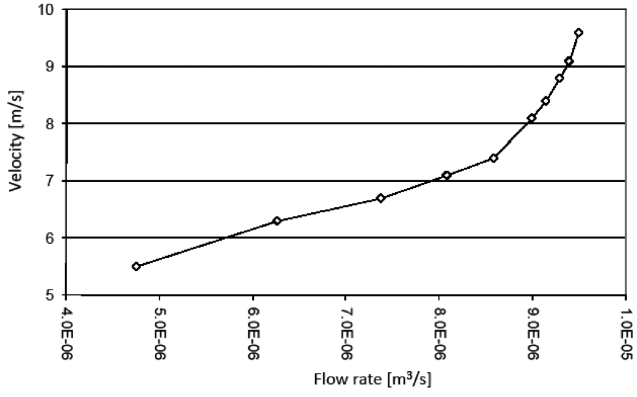

b)

Fig. 2 Single-nozzle characterization: a) average droplet diameter vs volumetric flow rate and b) droplet velocity vs volumetric flow rate.

minimizing stresses. Separating the heater from the phenolic base was a thin bed of silicon high-temperature RTV. This attachment method was considered to be optimal because the heater was allowed to expand or contract during heating and cooling without the need for a fixed mount that could induce a crack or other failure.

The chamber was instrumented with 10 type E thermocouples as well as a pressure transducer. Thermocouples were placed in the inlet and both outlet lines of the chamber as well as inside the aluminum containment foam that read an average chamber temperature, which was used to determine saturation conditions within the chamber. Two additional thermocouples were drilled at specific depths beneath the heater surface to calculate the heat loss through the phenolic base, which was not associated with spray cooling. The last three thermocouples, directly touching the bottom surface of the thick-film resistance heater, gave a rough temperature distribution across the backside of the heater, supplying temperature uniformity data associated with array spray interactions. Three type E miniature thermocouples, 0.508 mm in diameter, were fitted into individual machined channels to allow the heater to sit flat on the phenolic. The end of each interface thermocouple was bent to allow direct contact to the bottom of the heater substrate. In addition, an epoxy was used to fix the thermocouple tip to the heater bottom to prevent thermocouple repositioning during thermal expansion. Two additional type E thermocouples protruded into the chamber to measure average surrounding fluid temperatures.

An accurate surface temperature measurement was required to evaluate spray cooling performance. To avoid disturbing the flow across the surface of the heater, three type E thermocouples were positioned on the bottom of the heater to calculate an average temperature on the bottom of the heater. Elston [32] completed a one-dimensional heat conduction analysis using the heater materials and thicknesses from Table 1. A functional relationship was generated to determine the heater surface temperature T_{surf}, as shown in Eq. (1). The heat loss fraction f, the percentage of the heat lost through the bottom of the heater and not removed via the spray, was determined

Table 1 Thick-film resistor-layer information [19]

Layer	Position	Thickness, mm	Thermal conductivity, W/(m · K)
Ceramic substrate	Bottom	$L_c = 0.634$	$k_c = 27$
Resistive layer	Middle	$L_r = 0.008$	$k_r = 1.04$
Glass cover	Top (sprayed surface)	$L_g = 0.040$	$k_g = 1.04$

by analyzing steady-state heat transfer data obtained during baseline (terrestrial) testing [32]. This fraction was approximated by a linear relationship with heater input power, shown in Eq. (2), with a maximum heat loss of approximately 5.2%.

$$T_{\text{surf}} = \frac{Q}{A}\left(-\frac{(1-f)L_g}{k_g} - \frac{L_r}{2k_r} + \frac{fL_r}{k_r} + \frac{fL_c}{k_c}\right) + \bar{T}_{\text{int}} \qquad (1)$$

$$f = -0.00016101Q + 0.05239716 \qquad (2)$$

The purpose of the reservoir, shown in Fig. 3, was to contain excess fluid, reduce the pressure surges associated with pumping, and isolate the vapor from the transport lines feeding the nozzle pump. It consisted of a transparent container with an inlet at the top and an exit at the bottom. The most important component of the reservoir was the internal liquid–vapor separator, which was a structure consisting of very high surface area vanes that contained the liquid flow, and the vapor was forced radially outward. The vapor resided along the outer walls of the chamber, and the liquid was pulled out of the central-axis exit port and pumped to the array nozzles. Elston [32] performed a qualitative analysis on the performance of the liquid–vapor separator in microgravity.

Figure 4 shows the flow-loop schematic for the experiment. The liquid exited the reservoir and entered a magnetically coupled positive-displacement gear pump (Tuthill Corp.). The liquid was then pumped through a 15 μm in-line filter before it reached a turbine flow meter. After the flow meter, the liquid passed by a pressure transducer, which measured the pressure at the inlet of the 16-nozzle array. An in-line pressure switch cut off power to the entire system upon an overpressure spike of 690 kPa. An electrically actuated three-way bypass valve allowed liquid to either flow through or bypass the preheater and the 16-nozzle array. Under normal operation, the bypass valve was set to allow flow through a 12.7-mm-diam, 305-mm-long tubular preheater, which was fabricated using copper pipe wrapped with a nichrome heater wire and covered in fiberfrax insulation. The preheater contained a twisted metal ribbon that more efficiently heated the liquid before the nozzle inlet. The preheater was used to heat the liquid to vary the subcooling before it entered the nozzle array. Next, liquid entered the spray chamber through a 6.35 mm stainless steel tube and exited via two 12.7 mm stainless steel tubes that were at a reduced pressure. Immediately after exiting the chamber, the liquid was directed through a series of three liquid–air heat exchangers (Lytron Corp.). Just downstream of the heat exchangers resided a scavenge pump, with a pressure transducer on either side, which fed two-phase fluid into a 140 μm filter and finally back to the reservoir. The scavenge pump worked with the nozzle pump mentioned earlier to generate a push–pull system that created some redundancy as well as reliability and controllability.

The working fluid, 3M Fluorinert FC-72, was chosen because of its low toxicity level, dielectric property, and low boiling point (56°C at 1 atm). Although the amount of dissolved air in FC-72 can reach nearly 50% by volume, the amount of air was varied between $10.1 \leq C \leq 16.8\%$. Elston [32] presented the method used for determining the amount of air in the system by using Aire-ometer measurements gathered via FC-72 sample extraction. The amount of dissolved air was reduced using a vacuum-based membrane filter attached to the system. If the amount of dissolved air was too low, ambient air was bled into the system, allowed to reach equilibrium throughout the system, and the air content was measured again.

The data acquisition system consisted of a laptop computer connected to a data acquisition board (Agilent model 34970A). The various instrumentation devices used for this experiment were thermocouples, pressure transducers, flow meters, voltmeters, precision resistors (to accurately measure current via voltage drop), and an accelerometer. In addition to the data acquisition board, a calibrated reference point (Hart Ice Point Calibrator model 9101) for

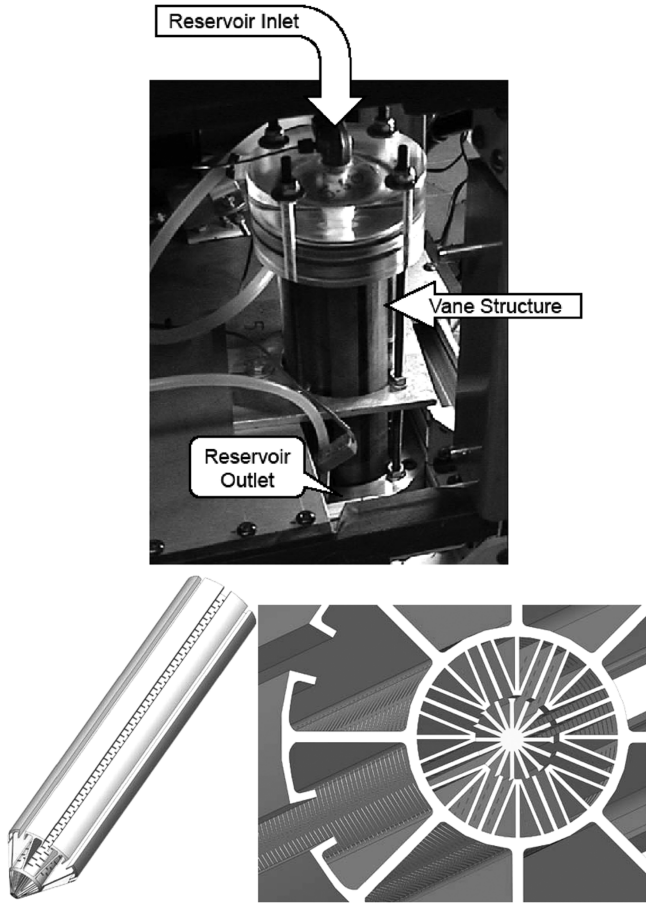

Fig. 3 Working-fluid reservoir and the internal liquid–vapor separator.

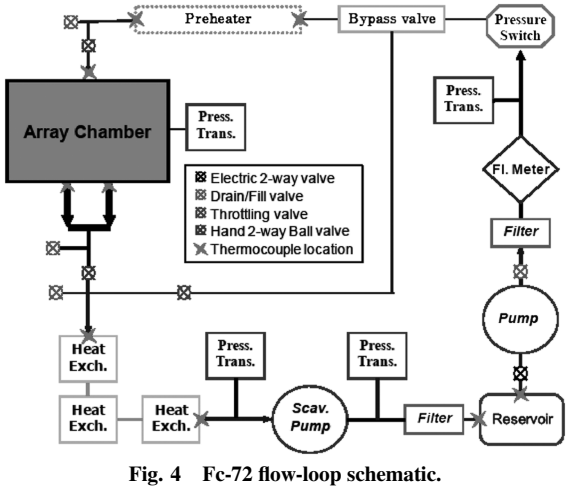

Fig. 4 Fc-72 flow-loop schematic.

the thermocouples was used, rather than the data acquisition system's built-in reference. This allowed for a steady-state thermocouple reference with a stability of ±0.005°C. The data acquisition software used the manufacturer's calibration information for the accelerometer, voltmeters, precision resistor, flow meters, and pressure transducers.

An uncertainty analysis was performed to be able to accurately report the data and determine the error ranges. The uncertainty was made up of precision error and bias error. Elston [32] summarized the precision error included in this experiment as the uncertainty associated with the instruments used to record the data, including the associated calibration error. The bias error was due to the scatter of the data and was calculated using the methodology contained in [34].

The precision error associated with the flow meter, thermocouples, heat flux, accelerometer, pressure transducers, and air content are summarized in Table 2. The thermocouple precision error was taken from the thermocouple calibration using a resistance temperature detector and readout (Hart Scientific models 5628 and 1502A), temperature bath (Hart Scientific model 6330), and the data acquisition system. The uncertainty associated with each device as well as the maximum deviation from the linear curve-fit were combined to generate the temperature precision error. The heat flux was estimated via two voltage measurements. The first voltage was measured across the resistive heating element, in which the uncertainty in this reading was only that associated with the data acquisition system. The second measured voltage was across a precision resistor in series with the heater. This was used to calculate the electrical current through the heater with errors associated with the data acquisition voltage measurement and the precision resistor uncertainty. The heater area was calculated by measuring the length and width using calipers; therefore, the uncertainty was that associated with the calipers. Finally, the precision errors associated with the accelerometer, pressure transducers, flow meter, and air content were assumed to be as stated by the manufacturer.

The bias error was the deviation in the data sets. The microgravity and 1.8 g portions of each parabola consisted of only 8 to 14 data points that included some data scattering. To report this scatter, the small groups of data were taken as an average data point plus or minus 1 standard deviation of the data.

Table 2 Summary of the uncertainty analysis

Type[a]	Error
T	
RTD	±0.006°C
RTD readout	±0.009°C
Curve-fit	±0.063°C
Total precision error	±0.078°C
Bias error σ	±0.63°C
q''	
Voltage 1 (DAQ)	±0.062 V
Voltage 2 (DAQ)	±0.0055 V
Resistor	±0.00002 Ω
Heater length	±0.000025 m
Heater width	±0.000025 m
Total precision error	±0.26 W/cm^2
Bias error σ	±0.00015 W/cm^2
$\dot{m}$	
Manufacturer	±0.039 g/s
Curve-fit	±0.66 g/s
Total precision error	±0.69 g/s
Bias error σ	±0.31 g/s
a	
Manufacturer	±0.025 g
Total precision error	±0.025 g
Bias error σ	±0.02 g
P	
Manufacturer	±1.72 kPa
Total precision error	±1.72 kPa
Bias error σ	±1.11 kPa
C	
Manufacturer	±2.0%
Total precision error	±2.0%
Bias error σ	±1.3%

[a]RTD denotes resistance temperature detector and DAQ denotes data acquisition system; bias error σ is from example case 01.

Flight tests with the 16-nozzle array were completed using NASA's C-9 reduced-gravity aircraft, which performed parabolic flight trajectories to control the acceleration field seen onboard. Two full flight weeks of testing were completed at NASA Johnson Space Center's Ellington Field. Each flight week consisted of four flights, usually one per day. Each flight consisted of a short amount of time after takeoff to travel to the approved flight zone, which allowed time for some experimental setup before the 46 parabolas would take place. Each parabola consisted of approximately 25 s of microgravity and 30 s of elevated gravity. In addition to the standard parabolas, 2.0 g turns were requested after each set of 10 parabolas so that the experiment would have enough time at an elevated gravity to reach steady state at several heater power settings.

Five parameters that were varied throughout the course of the flight weeks were acceleration a, heater power Q, mass flow rate $\dot{m}$, subcooling $\Delta T_{sc} = T_{sat} - T_{in}$, and air content C. During each parabolic maneuver, a heater power was set. Typically, this setting was maintained for two to three parabolas to achieve some repeatability in the data. During a group of parabolas, usually 10 or 20, the flow rate and subcooling were maintained constant, and only the heater power was varied. The flow rate and subcooling settings would only be adjusted once or twice over the course of an entire flight so that the effects of acceleration on heat transfer could be investigated.

III. Results and Discussion

The objective of the 16-nozzle array flight-test experiment was to show the effects of elevated or reduced gravity, mass flow rate, liquid subcooling, and dissolved air content on array spray cooling performance. To simplify the analysis, each flight was broken up into a series of cases, as shown in Table 3. Each case, defined as a portion of the flight in which the only parameter adjusted was the heater power, provided a means to look at the data in such a way that minimized the effects of the other parameters.

To investigate the effect of gravity on spray cooling performance, the experimental conditions were held constant as the plane went through a variable-gravity maneuver (parabola). During each parabola, the heater power, mass flow rate, subcooling, and air content were held constant, whereas the acceleration changed from microgravity to elevated gravity. After approximately two or three parabolas, the heater power was increased approximately 5 to 10 W. This pattern was repeated until the spray cooling system was near CHF, at which point the heater power was reduced and then increased in small steps to examine the behavior of the system near CHF while undergoing gravitational transients.

Figures 5 and 6 show how the experiment was operated and examines how the cooling performance was impacted by changes in acceleration. Figures 7–12 show the surface superheat dependence on acceleration, mass flow rate, degree of subcooling, and dissolved air content in both an elevated and a microgravity environment.

An example data set, shown in Fig. 5a, depicts the data collected during seven parabolas. The acceleration a is shown toward the bottom of the plot with the axis on the right-hand side, in which microgravity is shown to be near $a = 0.0$ g and elevated gravity is shown near $a = -2.0$ g (note that the acceleration shown is strictly the magnitude of the vector pointing in the same direction as the spray, normal to the heated surface). The mass flow rate is shown toward the top of the graph with the axis on the right-hand side. The heat flux transferred to the spray was incremented as follows: $(1 - f)q'' = 2.90$, 5.89, 8.88, and 11.8 W/cm^2. In this case, two parabolas at each heater setting were recorded before the next increment in heat flux. The subcooling and air content were both held constant during this block of data. As expected, the heater surface temperature T_{surf} increased with heat flux. However, T_{surf} showed a significant dependence on acceleration. Looking in more detail at the section between times A and B in Fig. 5a, with minimal flow rate fluctuations, a constant heat flux, and a transition from elevated

Table 3 Nominal parameter values

Case no.	$\dot{m}$, g/s	ΔT_{sc}, °C	T_{sat}, °C	$-a$, g	C, %
1	14.0	14.2	42.1	0.02	10.1
2	14.1	11.3	41.6	0.98	10.1
3	13.8	12.6	40.7	1.87	10.1
4	14.0	14.2	41.2	1.92	10.1
5	18.0	15.1	42.3	0.02	10.1
6	18.2	13.6	41.4	1.00	10.1
7	17.7	12.9	40.5	1.86	10.1
8	18.0	14.6	40.9	2.02	10.1
9	21.3	15.3	43.4	0.02	10.1
10	21.2	13.9	40.9	1.05	10.1
11	21.1	12.7	41.3	1.88	10.1
12	20.9	14.8	40.6	1.89	10.1
13	14.5	18.4	39.7	0.02	10.1
14	14.5	18.0	39.9	1.00	10.1
15	14.0	16.1	37.4	1.88	10.1
16	14.1	18.1	39.9	1.90	10.1
45	13.1	6.39	43.0	0.01	14.3
46	13.7	3.01	42.4	0.99	14.3
47	13.5	4.86	41.7	1.77	14.3
49	16.4	9.86	42.8	0.01	14.3
50	18.3	9.58	42.6	1.01	14.3
51	17.6	8.93	41.8	1.78	14.3
52	18.0	8.88	41.8	2.00	14.3
53	14.1	12.4	43.4	0.01	14.3
54	14.7	11.0	42.6	0.98	14.3
55	14.7	11.2	42.3	1.75	14.3
56	15.3	11.5	41.8	1.85	14.3
57	15.5	15.5	45.0	0.01	14.3
58	18.5	16.9	46.5	1.02	14.3
59	18.5	15.9	45.3	1.74	14.3
61	13.5	17.8	46.1	0.01	16.8
62	13.7	14.5	44.8	1.01	16.8
63	14.0	16.0	44.7	1.86	16.8
64	14.5	15.7	43.8	1.92	16.8
65	16.5	17.9	46.0	0.01	16.8
66	17.0	16.8	45.3	0.98	16.8
67	17.6	16.9	45.3	1.84	16.8
68	18.2	17.0	45.4	1.88	16.8
69	13.7	8.96	47.2	0.01	16.8
70	13.8	8.29	45.3	0.98	16.8
71	13.7	7.71	45.5	1.72	16.8
73	17.4	9.86	46.6	0.01	16.8
74	17.9	7.65	45.1	1.04	16.8
75	18.3	7.86	45.4	1.70	16.8

gravity to microgravity, the cooling performance was enhanced, resulting in a surface temperature reduction of approximately 13°C, which was similar to the degree of subcooling ($\Delta T_{sc} = 11.8 \pm 1.9$°C). Also, between times C and D, a similar enhancement, with a surface temperature reduction of approximately 15°C, was noted at a higher heat flux. In fact, the surface temperature decreased during each transition to microgravity and then increased under elevated gravity. This performance dependence on acceleration was witnessed by others: Yerkes et al. [29] and Michalak et al. [30] both showed a decrease in surface temperature in microgravity over terrestrial and elevated gravity.

Figure 5b displays the data traces of two parabolas with the heater input set to a higher value of $(1 - f)q'' = 20.5$ W/cm^2. Initially, the acceleration was $a = -1.91$ g, and the surface temperature was constant at approximately $T_{surf} = 71$°C. At point E, the aircraft experienced a transition to microgravity, at which time the surface temperature increased dramatically. When the interface temperature reached $T_{int} = 120$°C, a temperature-activated relay opened the heater circuit, thereby disconnecting power to the heater, preventing damage to the heater. This type of event is indicative of CHF, in which a runaway surface temperature is experienced. After the heater power was turned off, the spray continued to cool the heater surface until the temperature fell below the limit on the relay, at which time the heater was reenergized at the same heat input before the event. The data acquisition cycle time was approximately 2.2 s and therefore the temperature could surpass the relay trip point and fall before the data acquisition unit could record an interface temperature exceeding 120°C. After point F, where the acceleration field was steady at $a = -0.01$ g, the system returned to equilibrium, where the surface temperature decreased to a significantly lower level ($T_{surf} = 62$°C). It is interesting to note that before point E, when $a = -1.91$ g, CHF had not been reached. It was only during the transition from elevated gravity to microgravity that a CHF event was tripped. When the aircraft transitioned from microgravity back to elevated gravity (point G), a CHF event once again occurred until the point at which the acceleration became steady at $a = -1.91$ g (point H). At this time, the system again reached equilibrium and the surface temperature reached the previous level ($T_{surf} = 71$°C). However, after a short time, the surface temperature again suddenly increased (point I). This shows that the heat input of $(1 - f)q'' = 20.5$ W/cm^2 was indeed very close to CHF for $a = -1.91$ g and possibly tripped CHF as a result of small perturbations in acceleration. This behavior was deemed to be in a metastable region, in which small changes in the acceleration field can result in either stable operation or a CHF event. At point J, the aircraft again experienced steady microgravity, and after the heater was reenergized, the system returned to equilibrium, where the surface temperature settled back to the previous temperature of $T_{surf} = 62$°C. Again upon transition from microgravity to elevated gravity (point K), another CHF event occurred, repeating the behavior seen at point G.

Figure 6a presents the heat flux convected away from the surface vs the difference between the heater surface temperature and the saturation temperature of the working fluid, FC-72. Positive values of $T_{surf} - T_{sat}$ indicate two-phase heat transfer, whereas negative values indicate single-phase heat transfer (this demarcation declares that

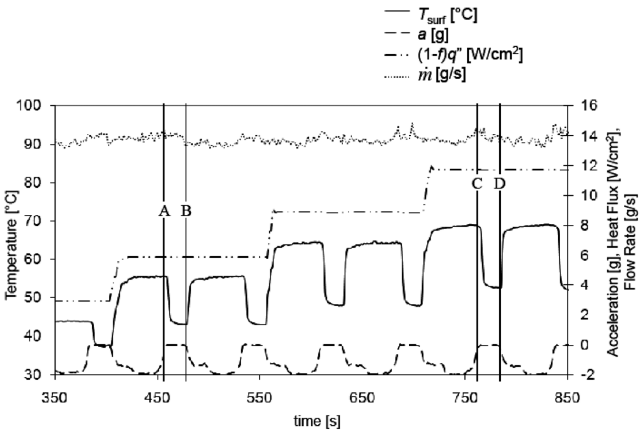

a)

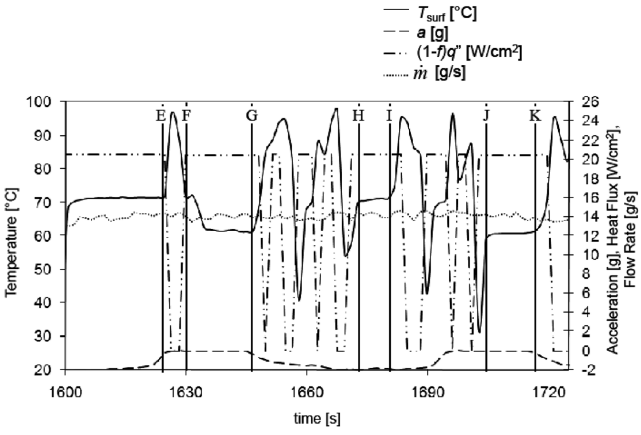

b)

Fig. 5 Transient data traces of surface temperature, acceleration, heat flux, and nozzle mass flow rate ($\dot{m} = 13.8 \pm 0.32$ g/s, $\Delta T_{sc} = 11.8 \pm 1.9$°C, and $C = 10.1\% \pm 1.3\%$): a) stable operation and b) CHF events ($(1 - f)q'' = 21.2 \pm 0.04$ W/cm^2).

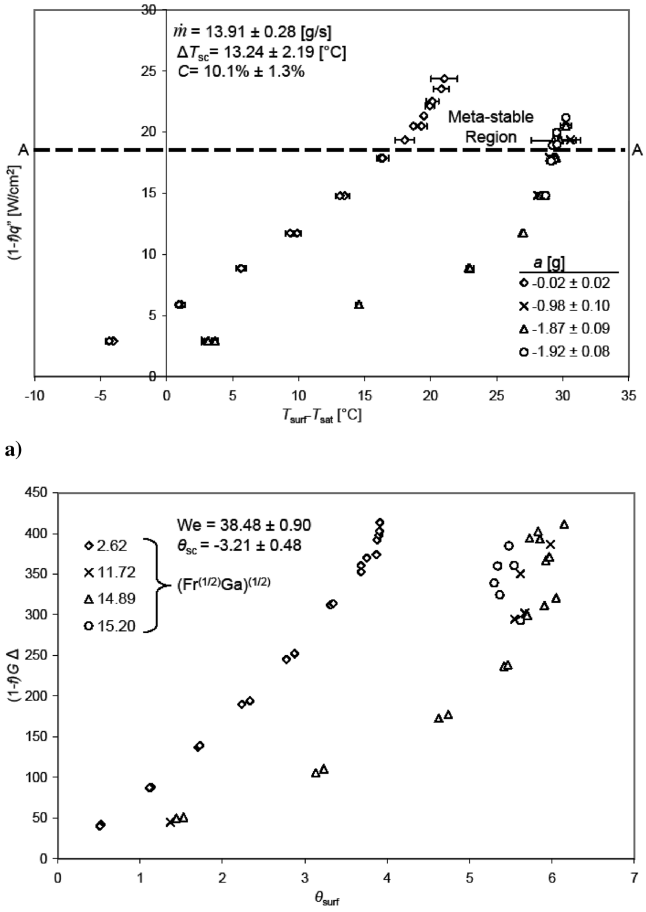

Fig. 6 Steady-state heat flux vs surface superheat ($\dot{m} = 13.91 \pm 0.28$ g/s, $\Delta T_{sc} = 13.24 \pm 2.19$°C, and $C = 10.1\% \pm 1.3\%$): a) dimensional values and b) dimensionless values.

only single-phase heat transfer takes place for negative values, but single-phase heat transfer can also occur at low positive wall superheat values in which the liquid is superheated and nucleation has not begun). In general, the temperature difference increased with heat flux until CHF was approached. Near this point, the temperature difference did not change appreciably. This behavior is typical of the two-phase process for spray cooling [7,20–22,25,26]. Of particular interest in this figure is the behavior of the data with respect to gravity: For terrestrial and elevated gravity ($a = -0.98$, -1.87 and -1.92 g), the results were nearly identical. For microgravity, however, the surface superheat was much less at a given heat flux, indicating a significant enhancement in heat transfer in microgravity. CHF was also higher (by approximately 3 W/cm^2) for microgravity than for terrestrial and elevated gravity.

The performance enhancement in microgravity could be explained by the fluid management system, in which the fluid was more easily wicked away from the surface in the absence of gravity, allowing for deeper spray penetration, suggesting that the performance enhancement may have been due to the test apparatus design in coordination with microgravity operation. Yerkes et al. [29] saw a similar trend, but at a much smaller magnitude using a single nozzle and no immediate wicking structure, suggesting that, to a certain degree, the performance enhancement was due strictly to the absence of a gravitational field. Figure 6a also illustrates the previously mentioned metastable region, which occurs above a certain heat flux threshold. Transients from gravitational forces drive the system to an onset of CHF, resulting in a sudden temperature increase for a constant heat flux. The horizontal line A–A designates the maximum heat flux that does not show the behavior induced by gravitational transients. Any heat flux above this line could potentially reach CHF in a transient acceleration environment. If the acceleration was stable, the critical heat flux when $a = -0.98$, -1.87, and -1.92 g was near $q = 22$ W/cm^2, whereas CHF when $a = -0.02$ g was near $q = 25$ W/cm^2. Metastability poses a significant problem if an aircraft system is designed to be in that metastable region: premature CHF can occur and lead to catastrophic device failure.

Figure 6b examines the data in Fig. 6a by casting it in the nondimensional terms suggested by Yerkes et al. [29]. For a constant $(1-f)G\Delta$ the dimensionless temperature θ was significantly different when $(Fr^{1/2}Ga)^{1/2}$ was varied. Also, for the higher values of $(Fr^{1/2}Ga)^{1/2}$, the dimensionless surface temperature was less dependent on $(Fr^{1/2}Ga)^{1/2}$.

The effect of acceleration on the temperature difference between the surface and saturation is shown in Fig. 7, in which each line represents a different heat flux. Figure 7 shows that the surface superheat at terrestrial and elevated gravity was very similar, exhibiting no significant variation due to gravitational body forces. In microgravity, however, a dramatic surface temperature drop occurred, displaying a significant performance enhancement. The microgravity cooling performance enhancement obtained agrees with the trends found by Sone et al. [25], Yoshida et al. [26], Baysinger et al. [27], Baysinger [28], Yerkes et al. [29], and Michalak et al. [30].

Figure 8 presents the surface superheat for three nominal mass flow rates $\dot{m} = 14.0$, 17.5, and 21.0 g/s. In Fig. 8a, in which $a = -0.02$ g, the surface superheat decreased slightly and then increased significantly with mass flow rate. This increase in the superheat was more pronounced as the heat input increased. In general, a decrease in the surface superheat with increasing mass flow rate is expected, due to the increased impact velocity of the droplets. The dramatic increase in the surface superheat at the highest flow rate may be due to liquid buildup in the array nozzle interaction zones, as described by Glassman et al. [5]. Figure 8b shows the surface superheat under elevated gravity ($a = -1.72$ g). The decrease in the superheat with increasing mass flow rate is again noted, but the sudden increase in the superheat was not present in this case. This may be due to an improvement in the ability of the liquid to exit the heater surface, which was provided by the body force on the liquid. This somewhat reinforces the assumption that the sudden increase seen in Fig. 8a was due to liquid buildup on the heater surface. It is possible that a similar increase in the superheat would also be seen for the elevated-gravity case at higher mass flow rates.

Figure 9 also illustrates the aforementioned cooling performance due to variation in mass flow rate. Figure 9a shows that when the mass flow rate was increased from $\dot{m} = 14.0$ to 17.5 g/s, a similar surface superheat reduction occurred for both elevated and microgravity. Figure 9b shows that when the mass flow rate was increased from $\dot{m} = 14.0$ to 21.0 g/s, the surface temperature decreased in elevated gravity but increased in microgravity, as shown in Fig. 8. It is important to note that even though cooling performance degradation was seen in microgravity, the surface superheat was still lower than the elevated-gravity case at the same flow rate. The

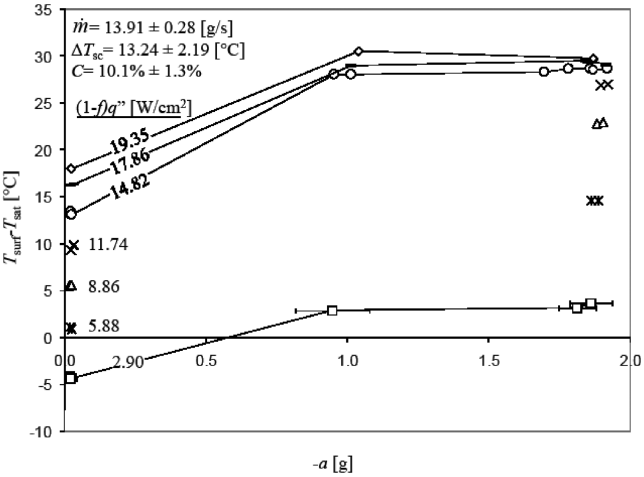

Fig. 7 Effect of acceleration on surface superheat ($\dot{m} = 13.91 \pm 0.28$ g/s, $\Delta T_{sc} = 13.24 \pm 2.19$°C, and $C = 10.1\% \pm 1.3\%$).

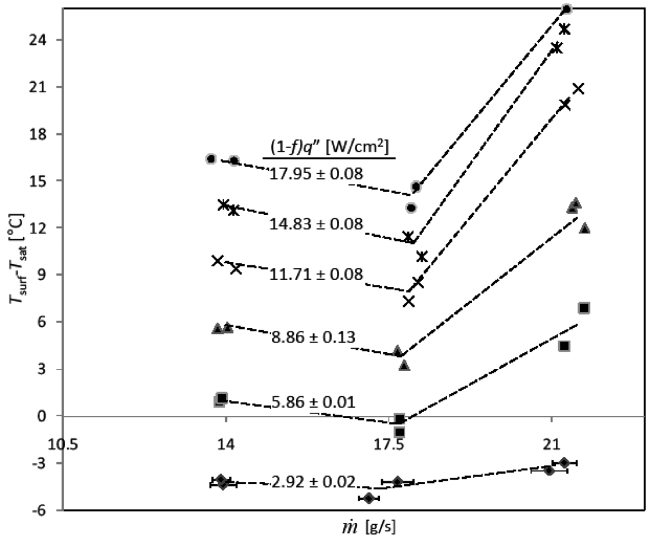

a)

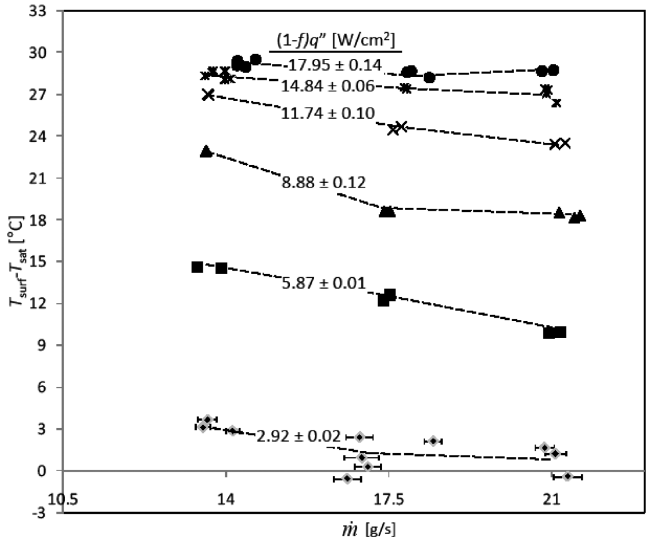

b)

Fig. 8 Effect of flow rate on the surface superheat ($\Delta T_{sc} = 13.7 \pm 2.3$°C and $C = 10.1\% \pm 1.3\%$): a) $a = -0.02 \pm 0.01\ g$ and b) $a = -1.72 \pm 0.34\ g$.

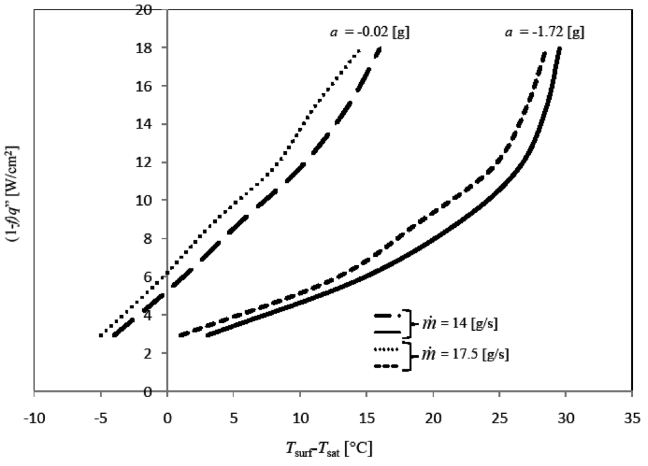

a)

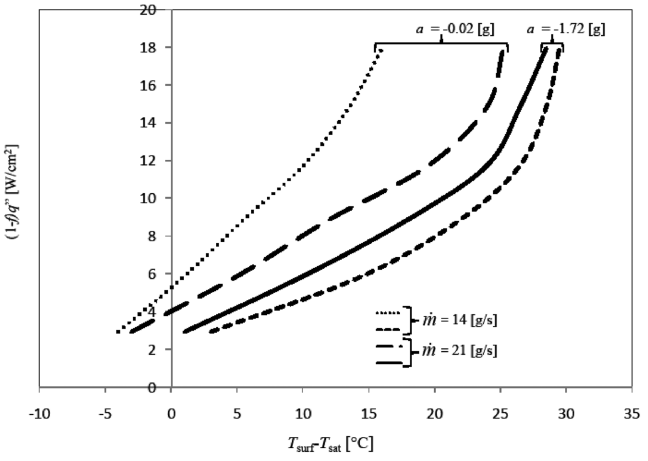

b)

Fig. 9 Effect of flow rate and acceleration on the cooling performance in elevated and microgravity ($\Delta T_{sc} = 13.7 \pm 2.3$°C and $C = 10.1\% \pm 1.3\%$): a) $\dot{m} = 14.0$ and 17.5 g/s and b) $\dot{m} = 14.0$ and 21.0 g/s.

reduction in cooling performance in microgravity due to a high mass flow rate was most likely due to excessive liquid buildup on the heater surface, preventing the deep penetration of droplets that occurred in the lower flow rate cases. The microgravity cooling performance enhancement seen at lower flow rates diminishes at higher flow rates, suggesting that as the mass flow continues to increase, the cooling performance in microgravity would not be appreciably different than in elevated gravity.

Figure 10 shows the effect of liquid subcooling on the surface superheat. This case is for a mass flow rate of $\dot{m} = 14.0$ g/s, which, as shown in Fig. 8, is not affected by liquid buildup on the heater surface. For the microgravity case (Fig. 10a), the surface superheat decreased with increasing subcooling for all values of heat input. In fact, it appears that the slope of the heat flux lines is nearly constant throughout for the microgravity case. In the elevated-gravity case shown in Fig. 10b, however, the slope of the surface superheat with respect to subcooling varies with heat input: at low heat flux values, the surface temperature drops as subcooling increases, but at high flux values, the surface superheat is nearly constant over the range tested. The physical mechanisms related to the heat transfer improvement are not well understood.

Figure 11 presents the effect of subcooling on the cooling performance in both elevated and microgravity. The four curves on the left-hand side of the plot were taken from microgravity test data and the three curves on the right-hand side were taken from elevated-gravity test data. In elevated gravity, there was little change in the cooling performance due to variation in the degree of subcooling, as seen in Fig. 10b The microgravity curves show that an increase in subcooling translated to a steady decrease in the surface superheat, as shown in Fig. 10a. Also note that as the amount of subcooling decreases in microgravity, the cooling performance curve nears that of the elevated-gravity case, suggesting that when the degree of subcooling approaches zero, the cooling performance enhancement seen in microgravity diminishes.

FC-72 has the capability of absorbing up to 48% air by volume. It was suspected that the effect of dissolved air may have also impacted the cooling performance in microgravity [29]. However, because air molecules are small enough to fit interstitially, the density change is less than 0.1% between air-saturated and degassed FC-72. It was not clear what effect absorbed air had on heat transfer in elevated or microgravity. Puterbaugh et al. [14] and Puterbaugh [15] determined that there was no significant variation in CHF due to dissolved air in FC-72 when saturation pressure was held constant. This suggested that the effect seen by previous researchers could have been a result of varying saturation pressure.

Figure 12 shows the effect of air content on the surface superheat, in which values of $C = 10.1$, 14.3, and 16.8% were examined in microgravity and elevated gravity. Figure 12a shows a slight decrease in the surface superheat with increasing air content, especially at lower heat flux values. Figure 12b, however, shows that the surface superheat increased slightly with air content in elevated gravity. This variation is considered to be within experimental uncertainty and

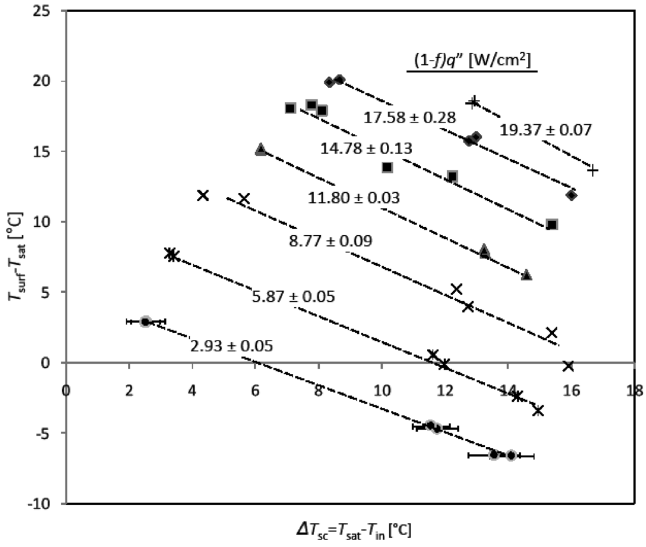

a)

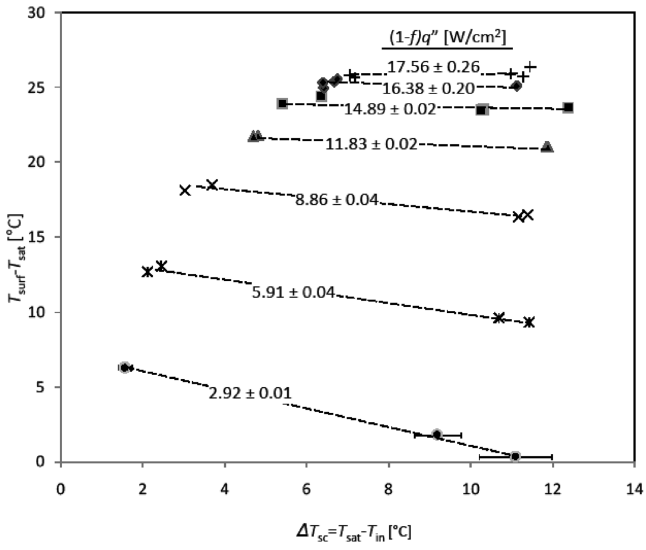

b)

Fig. 10 Effect of subcooling on the surface superheat ($\dot{m} = 14.0 \pm 0.93$ g/s and $C = 14.3\% \pm 2.2\%$): a) $a = -0.01 \pm 0.01\ g$ and b) $a = -1.75 \pm 0.03\ g$.

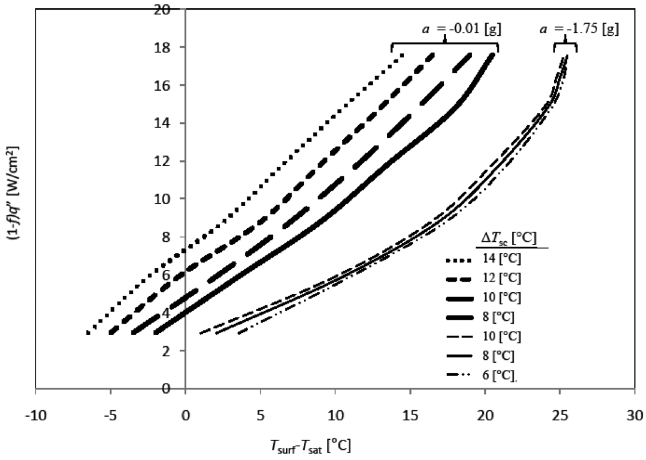

Fig. 11 Effect of subcooling and acceleration on cooling performance in elevated and microgravity ($\dot{m} = 14.0 \pm 0.93$ g/s and $C = 14.3\% \pm 2.2\%$).

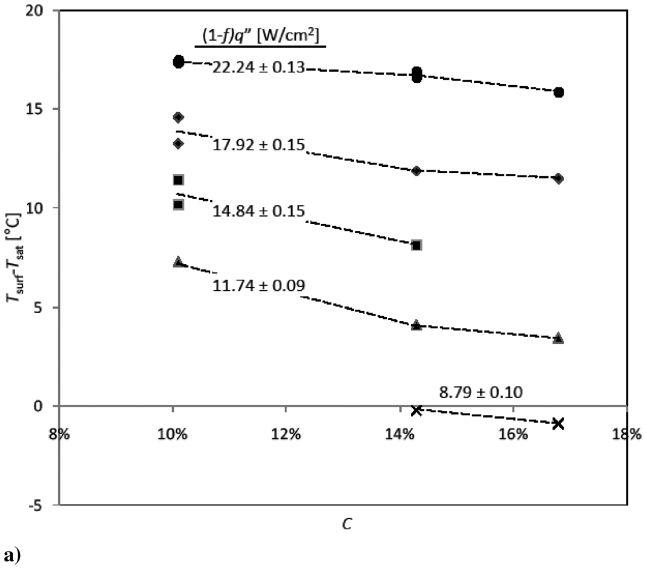

a)

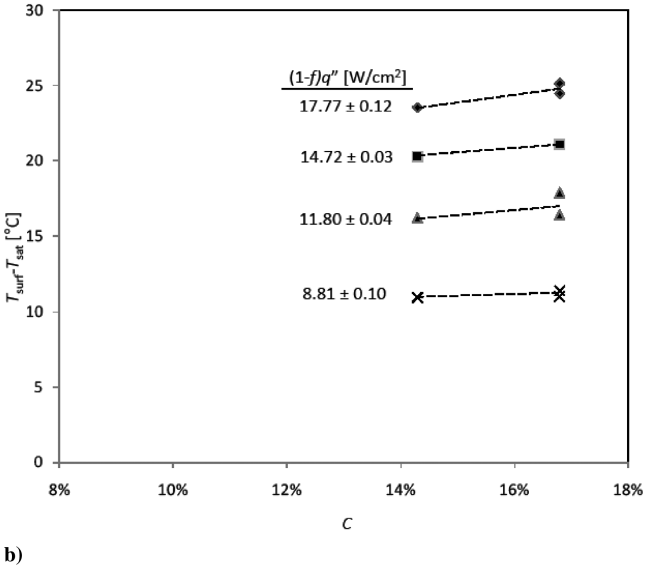

b)

Fig. 12 Effect of air content on the surface superheat ($\Delta T_{sc} = 16.7 \pm 1.1$°C, $\dot{m} = 17.4 \pm 0.95$ g/s): a) $a = -0.01 \pm 0.01\ g$ and b) $a = -1.69 \pm 0.31\ g$.

quite small in comparison with the effects of acceleration, mass flow rate and liquid subcooling.

IV. Conclusions

The effects of variable gravity on the spray cooling performance of a 16-nozzle array using FC-72 were investigated. An experimental apparatus previously flown on NASA's reduced-gravity aircraft was modified to accommodate the 16-nozzle array chamber with a 25.4 × 25.4 mm^2 heater. The reduced-gravity portions of the flight test showed a very repeatable surface temperature reduction from the terrestrial- and elevated-gravity portions. The effects of acceleration, mass flow rate, degree of subcooling, and air content on the cooling performance of the array were studied. In stable acceleration fields, microgravity exhibited a significant decrease in surface superheat over terrestrial gravity. Elevated gravity had no appreciable effect in surface superheat when compared with terrestrial gravity. Although the cooling performance appeared to be enhanced due to the reduction of body forces, the data suggest that for an aircraft that undergoes a transient variation of acceleration, a metastability condition can occur that will influence the onset of CHF. This can result in a runaway temperature condition, leading to electronic component damage or failure. The cooling performance was enhanced when the mass flow rate increased from $\dot{m} = 14.0$ to 17.5 g/s in both elevated

and microgravity, but the cooling performance was degraded when the mass flow rate increased from $\dot{m} = 17.5$ to 21.0 g/s in microgravity only. This was possibly due to liquid buildup in the nozzle interaction zones, in which the liquid thickness was much greater than that directly under the spray. An increase in subcooling dramatically decreased the surface superheat in microgravity for all heat fluxes evaluated. In elevated gravity, the subcooling reduced the surface superheat for low heat fluxes and had little effect at high heat fluxes. This may have been due to bubble dynamics on the heater surface. An increase in the amount of dissolved air in the working fluid decreased the surface superheat slightly in microgravity, but no significant effect was seen in elevated gravity. A larger variation in air content dissolved in the working fluid, FC-72, may have shown more of an effect.

Acknowledgments

This research was conducted as part of the in-house program at the U.S. Air Force Research Laboratory, Propulsion Directorate, Energy/Power/Thermal Division, Thermal and Electrochemical Branch, Wright–Patterson Air Force Base, Ohio.

References

[1] Mudawar, I., "Assessment of High-Heat-Flux Thermal Management Schemes," *IEEE Transactions on Components and Packaging Technologies*, Vol. 24, No. 2, 2001, pp. 122–141. doi:10.1109/6144.926375

[2] Lee, H. S., Merte, H., and Chiaramonte, F., "Pool Boiling Curve in Microgravity," *Journal of Thermophysics and Heat Transfer*, Vol. 11, No. 2, 1997, pp. 216–222. doi:10.2514/2.6225

[3] Gu, J., Kawaji, M., and Futamata, R., "Effects of Gravity on the Performance of Pulsating Heat Pipes," *Journal of Thermophysics and Heat Transfer*, Vol. 18, No. 3, 2004, pp. 370–378. doi:10.2514/1.3067

[4] Kim, J., "Review of Reduced Gravity Boiling Heat Transfer: US Research," *Journal of the Japan Society of Microgravity Application*, Vol. 20, No. 4, 2003, pp. 264–271.

[5] Glassman, B., Kuravi, S., Du, J., Lin, Y., Zhao, G., and Chow, L., "A Fluid Management System for a Multiple Nozzle Array Spray Cooler," 37th AIAA Thermophysics Conference, AIAA Paper 2004-2574, 2004.

[6] Kim, J., "Spray Cooling Heat Transfer: The State of the Art," *International Journal of Heat and Fluid Flow*, Vol. 28, No. 4, 2007, pp. 753–767. doi:10.1016/j.ijheatfluidflow.2006.09.003

[7] Ortiz, L., and Gonzalez, J. E., "Experiments on Steady-State High Heat Fluxes Using Spray Cooling," *Experimental Heat Transfer*, Vol. 12, 1999, pp. 215–233. doi:10.1080/089161599269690

[8] Johnson, J. E., Selvam, R. P., and Silk, E. A., "Spray Cooling Modeling: Droplet Sub-Cooling Effect on Heat Transfer," *AIP Conference Proceedings*, Vol. 969, American Inst. of Physics, New York, 2008, pp. 104–111.

[9] Selvam, R. P., and Ponnappan, R., "Numerical Modeling of Nucleation Boiling in Thin Film and Effect of Droplet Impact," *Proceedings of the 15th Annual Thermal and Fluids Analysis Workshop (TFAWS 2004)*, Jet Propulsion Lab., California Inst. of Technology, Pasadena, CA, 2004.

[10] Selvam, R. P., Lin, L., and Ponnappan, R., "Computational Modeling of Spray Cooling: Current Status and Future Challenges," *AIP Conference Proceedings*, Vol. 746, American Inst. of Physics, New York, 2005, pp. 55–63.

[11] Selvam, R. P., Sarkar, M., and Ponnappan, R., "Modeling of Spray Cooling: Effect of Droplet Velocity and Liquid to Vapor Density Ratio on Heat Transfer," *Proceedings of the 16th Annual Thermal and Fluids Analysis Workshop (TFAWS 2005)*, NASA Kennedy Space Center, Merritt Island, FL, 2005.

[12] Selvam, R. P., Sarkar, M., Sarkar, S., and Ponnappan, R., "Effect of Vapor Bubble Size in Heat Transfer in Spray Cooling," *AIP Conference Proceedings*, Vol. 813, American Inst. of Physics, New York, 2006, pp. 145–152.

[13] Selvam, R. P., Sarkar, S., and Ponnappan, R., "Modeling of Spray Cooling: Convective Flow Effect on Vapor Bubble Dynamics and Heat Transfer," 9th AIAA/ASME Joint Thermophysics Heat Transfer Conference, AIAA Paper 2006-3411, 2006.

[14] Puterbaugh, R. L., Yerkes, K. L., Michalak, T. E., and Thomas, S. K., "Cooling Performance of a Partially-Confined FC-72 Spray: The Effect of Dissolved Air," 45th AIAA Aerospace Sciences Meeting and Exhibit, AIAA Paper 2007-199, 2007.

[15] Puterbaugh, R. L., "The Effect of Dissolved Air on the Cooling Performance of a Partially-Confined FC-72 Spray," M.S. Thesis, Dept. of Mechanical and Materials Engineering, Wright State Univ., Dayton, OH, 2008.

[16] Kreitzer, P. J., and Kuhlman, J. M., "Visualization of Electro-hydrodynamic Effects and Time Scale Analysis for Impinging Spray Droplets of HFE-7000," *AIP Conference Proceedings*, Vol. 969, American Inst. of Physics, New York, 2008, pp. 86–93.

[17] Kreitzer, P. J., "Experimental Testing of Convective Spray Cooling with the Aid of an Electrical Field Using the Coulomb Force," M.S. Thesis, Dept. of Mechanical and Aerospace Engineering, West Virginia Univ., Morgantown, WV, 2006.

[18] Kreitzer, P. J., Kuhlman, J. M., Mehra, D., Gray, D., and Yerkes, K. L., "Effects of Contact Charging on Spray Impingement Heat Transfer Performance and Spray Behavior," 39th AIAA Thermophysics Conference, AIAA Paper 2007-4269, 2007.

[19] Glaspell, S. L., "Effects of the Electric Kelvin Force on Spray Cooling Performance," M.S. Thesis, Dept. of Mechanical and Aerospace Engineering, West Virginia Univ., Morgantown, WV, 2006.

[20] Chow, L. C., Sehmbey, M. S., and Pais, M. R., "Critical Heat Flux in Spray Cooling," 34th AIAA Aerospace Sciences Meeting and Exhibit, AIAA Paper 96-0727, 1996.

[21] Lin, L., and Ponnappan, R., "Heat Transfer Characteristics of Spray Cooling in a Closed Loop," *International Journal of Heat and Mass Transfer*, Vol. 46, No. 20, 2003, pp. 3737–3746. doi:10.1016/S0017-9310(03)00217-5

[22] Lin, L., and Ponnappan, R., "Two-Phase High Capacity Spray Cooling Loop: Nozzle Orientation Effects and Performance Results," 3rd AIAA International Energy Conversion Engineering Conference, AIAA Paper 2005-5733, 2005.

[23] Lin, L., Ponnappan, R., Yerkes, K. L., and Hager, B., "Large Area Spray Cooling," 42nd AIAA Aerospace Sciences Meeting and Exhibit, AIAA Paper 2004-1340, 2004.

[24] Lin, L., Harris, R., Lawson, J., and Ponnappan, R., "Spray Cooling with Methanol and Water Mixtures," 9th AIAA/ASME Joint Thermophysics and Heat Transfer Conference, AIAA Paper 2006-3410, 2006.

[25] Sone, K., Yoshida, K., Oka, T., Abe, Y., Mori, Y., and Nagashima, A., "Spray Cooling Characteristics of Water and FC-72 Under Reduced and Elevated Gravity for Space Application," *Proceedings of the International Energy Conversion Engineering Conference*, Vol. 2, 1996, pp. 1500–1505.

[26] Yoshida, K., Abe, Y., Oka, T., Mori, Y., and Nagashima, A., "Spray Cooling Under Reduced Gravity Condition," *Journal of Heat Transfer*, Vol. 123, No. 2, 2001, pp. 309–318. doi:10.1115/1.1345887

[27] Baysinger, K. M., Yerkes, K. L., Michalak, T. E., Harris, R. J., and McQuillen, J., "Design of a Microgravity Spray Cooling Experiment," 42nd AIAA Aerospace Sciences Meeting and Exhibit, AIAA Paper 2004-0966, 2004.

[28] Baysinger, K. M., "Experimental Testing and Numerical Modeling of Spray Cooling Under Terrestrial Gravity Conditions," M.S. Thesis, Dept. of Mechanical and Materials Engineering, Wright State Univ., Dayton, OH, 2005.

[29] Yerkes, K. L., Michalak, T. E., Baysinger, K. M., Puterbaugh, R., Thomas, S. K., and McQuillen, J., "Variable- Gravity Effects on a Single-Phase Partially Confined Spray Cooling System," *Journal of Thermophysics and Heat Transfer*, Vol. 20, No. 3, 2006, pp. 361–370. doi:10.2514/1.18681

[30] Michalak, T. E., Yerkes, K. L., Puterbaugh, R., Thomas, S. K., and McQuillen, J., "Cooling Performance of a Partially-Confined FC-72 Spray: The Effect of Variable Gravity," 45th AIAA Aerospace Sciences Meeting and Exhibit, AIAA Paper 2007-198, 2007.

[31] Gambaryan-Roisman, T., Kyriopoulos, O., Roisman, I., Stephan, P., and Tropea, C., "Gravity Effect on Spray Impact and Spray Cooling," *Microgravity Science and Technology*, Vol. 19, Nos. 3–4, 2007, pp. 151–154.

[32] Elston, L. J., "The Effect of Variable Gravity on the Cooling Performance of a 16-Nozzle Spray Array," M.S. Thesis, Dept. of Mechanical and Materials Engineering, Wright State Univ., Dayton, OH, 2008.

[33] Yaniec, J. S., and Del Rosso, D., "NASA JSC Reduced Gravity Program User's Guide," Aircraft Operations Div., Rept. AOD 33899, Houston, TX, 2007.

[34] Fox, R. W., McDonald, A. T., and Pritchard, P. J., *Introduction to Fluid Mechanics*, Wiley, New York, 2003.